



# Magnetohydrodynamic natural convection of hybrid nanofluid in a porous enclosure: numerical analysis of the entropy generation

Zaim Abdel-Nour<sup>1</sup> · Abderrahmane Aissa<sup>2</sup> · Fateh Mebarek-Oudina<sup>3</sup> · A. M. Rashad<sup>4</sup> · Hafiz Muhammad Ali<sup>5</sup> · M. Sahnoun<sup>2</sup> · M. El Ganaoui<sup>6</sup>

Received: 18 March 2020 / Accepted: 9 April 2020 / Published online: 27 April 2020  
© Akadémiai Kiadó, Budapest, Hungary 2020

## Abstract

The effect on the entropy production and MHD convection of the hybrid nanofluid  $\text{Al}_2\text{O}_3\text{-Cu/water}$  (water with Cu and  $\text{Al}_2\text{O}_3$  nanoparticles) in a porous square enclosure is studied numerically via Galerkin finite element method. The enclosure used for flow and natural convection analysis is subjected to sinusoidal varying temperatures at the boundaries. Calculations were performed for specific parameters of the Rayleigh number ( $\text{Ra} = 10^3\text{-}10^6$ ), porosity ratio ( $\varepsilon = 0.1\text{-}0.9$ ), Darcy number ( $\text{Da} = 10^{-5}\text{-}10^{-2}$ ), Hartmann number ( $\text{Ha} = 0\text{-}100$ ) and nanoparticles concentration ( $\varphi = 0\text{-}0.08$ ). The numerical results are presented by velocity profiles, isotherms, streamlines, and Nusselt number. They indicate that the isotherms subject to estimation variations under Ha boost from 0 to 100 as Ra enhances. At high Ha, the conduction transfer mechanism is more obvious. Also, it is seen that the convective heat transfer becomes stronger with the enhancement of the Ra while it detracts with the rise in Ha. Due to the Ra increase, the flow cell becomes stronger. For  $\text{Ra} = 10^6$  and higher Hartmann numbers, the isotherms remain constant which is an indication of convection predominance.

**Keywords** Entropy generation · Porous enclosure · Natural convection · Magnetic field · Hybrid nanofluid

## List of symbols

Nu Nusselt number  
Da Darcy number  
 $L$  Height of cavity (m)  
Pr Prandtl number  
 $P$  Pressure  
 $K$  Thermal conductivity ( $\text{W m}^{-1} \text{K}^{-1}$ )  
 $u, v$  Non-dimensional velocity components

$L_1$  Width of cavity (m)  
 $W$  Length of cavity (m)  
 $x, y$  Coordinate  
 $W_1$  Width of cavity (m)

## Greeks symbols

$\alpha$  Thermal diffusivity ( $\text{m}^2 \text{s}^{-1}$ )  
 $\beta$  Thermal expansion coefficient ( $\text{K}^{-1}$ )  
 $\theta$  Temperature  
 $\varepsilon$  Porosity  
 $\mu$  Dynamic viscosity ( $\text{kg m}^{-1} \text{s}^{-1}$ )  
 $\varphi$  Volume fraction  
 $\rho$  Density ( $\text{kg m}^{-3}$ )

## Superscripts

avg Average  
hnf Hybrid nanofluid  
c Cold  
loc Local  
s Solid particles

✉ Hafiz Muhammad Ali  
hafiz.ali@kfupm.edu.sa

<sup>1</sup> LSTE Laboratory, Faculty of Science and Technology, University of Mascara, Mascara, Algeria

<sup>2</sup> Laboratoire de Physique Quantique de la Matière et Modélisation Mathématique (LPQ3M), Université Mustapha Stambouli de Mascara, Mascara, Algeria

<sup>3</sup> Department of Physics, Faculty of Sciences, University of 20 août 1955-Skikda, Skikda, Algeria

<sup>4</sup> Department of Mathematics, Faculty of Science, Aswan University, Aswân 81528, Egypt

<sup>5</sup> Mechanical Engineering Department, King Fahd University of Petroleum and Minerals, Dhahran 31261, Saudi Arabia

<sup>6</sup> Laboratoire énergétique de Longwy (FJV/LERMAB), Université de Lorraine, Longwy, France

## Introduction

Heat transfer forms the origin of many industrial processes that are present in our daily life. The magnification of these exchanges and the improvement of the efficiency have become currently problematic in the industrial world, which turn out to be more conscious to the progressive collapse of energy resources. Confronted to these energy and environmental tasks, the technological challenge lies in the development of new processes for better energy controlling. Therefore, new optimization strategies must be studied. One of these strategies consists in improving the thermal properties of the heat transfer of the fluids used in thermal systems, in particular in heat exchangers. Significant progress in chemistry made it possible at the end of the 1990s to synthesize nanometric-sized particles, which, dispersed in a liquid carrier, constitute nanofluids [1–4]. Their synthesis comes upon the need to boost the thermal properties of fluids by inserting a solid phase with very high thermal conductivity such as metallic or metal oxide nanoparticles [5–7]. Heat transfer fluids can be gases, organic fluids, liquid metals, or water. Heat transfer fluids have been developed and used in a huge variety of applications. They are chosen according to the quantities required and their physicochemical properties, their thermal conductivity, their anticorrosive properties, their cost and their impact on the environment. Water is one of the most used because of its economy, its high thermal capacity and its high thermal conductivity.

Nanofluids are relatively a novel category of fluids which consist of a basic fluid with particles of nanometric size (1–100 nm), in suspension. Endowed with particular and interesting physicochemical properties, such as their high conductivity, nanofluids have an efficient thermal conductivity higher than that of base liquids [8–10]. Numerous researches have been conducted on the hydrothermal features of MHD, a phenomenon which is caused by the impact of magnetic fields on electrically conductive fluids [11, 12]. Mehryan et al. [13] have studied unsteady MHD natural convection inside an enclosure employing numerical simulation. Cavity is divided by an elastic film. The outcomes show that the variation in the Hartmann number affected the shape of the film and the heat transfer. Bahrami et al. [14] investigated numerically heat transfer enhancement inside an eccentric porous cylinder with an inner moving wall. They concluded that the insertion of porous supports with higher Darcy numbers improves heat transfer and its effect is very considerable for high Rayleigh numbers. Another research, Rashad et al. [15] studied the effectiveness of MHD convection in an enclosure. They reported that the Nusselt number declines with the Lorentz forces. Anjali et al. [16] investigated the

magnetoconvection over a porous stretchable sheet. They observed that the thermal performance of the hybrid nanofluid is greater than the conventional nanofluid with magnetic field environment. Afrand et al. [17] analyzed experimentally the impacts of volume fraction on heat transfer. With different volume fractions (0.0375–1.2%), stable and homogeneous suspensions have been prepared and viscosity measurements were reported as temperatures between 25 and 50 °C. Aman et al. [18] presented exact solutions for the investigation of improved various parameters of Casson fluid (alumina and copper nanoparticles). Ghalebaz et al. [19] have studied the conjugate free convection Ag–MgO in a porous enclosure using LTE analysis. The outputs show that the hybrid nanoparticles decline the heat transfer rate and flow strength. Mehryan et al. [20] studied the natural convection hybrid nanofluid within a porous cavity under magnetic field based on two-equation energy model. Mohebbi et al. [21] investigated the natural convection within a permeable enclosure for solar power plants.

Many researchers have recently reported a more interesting contribution on this subject using different numerical methods [33–39]. The main objective of these numerical studies is to find a solution to the problems encountered in industrial and thermal systems.

To the authors' best knowledge, from the previous recent literature review in this field no available paper at all deals with the entropy production due to MHD convection in an enclosure with a sinusoidal bottom and vertical wall which filled with hybrid nanofluid and porous media.

## Problem description

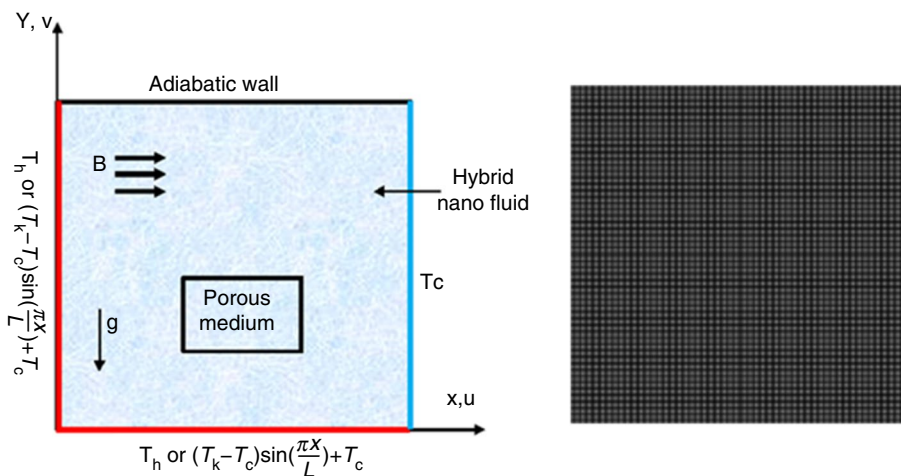
A schematic representation of free convection hybrid nanofluid flow in porous enclosure has been investigated in the present work (Fig. 1). The enclosure is heated sinusoidally from the bottom and right vertical wall where the top is adiabatic. The hybrid nanofluid flow considering laminar, incompressible and the external magnetic field is applied.

## Governing equations

The steady MHD convection hybrid nanofluid flow in a square enclosure is analyzed here. To model a porous medium, the Brinkman [22] model is used. Heat equations and Navier–Stokes are expressed in Cartesian coordinates for the problem by considering the above assumptions that can be expressed in the non-dimensional model as follows:

$$\frac{\partial U}{\partial X} + \frac{\partial V}{\partial Y} = 0 \quad (1)$$

**Fig. 1** The geometry Mesh distribution for the physical model



$$U \frac{\partial U}{\partial X} + V \frac{\partial U}{\partial Y} = -\frac{\partial P}{\partial X} + \text{Pr} \left( \frac{\partial^2 U}{\partial X^2} + \frac{\partial^2 U}{\partial Y^2} \right) - \frac{\text{Pr}}{\text{Da}} U + \text{Ha}^2 \text{Pr} U \quad (2)$$

$$S_T = S_\psi + S_\theta + S_C + S_M \quad (9)$$

Using the following change of variables,

$$U \frac{\partial V}{\partial X} + V \frac{\partial V}{\partial Y} = -\frac{\partial P}{\partial Y} + \text{Pr} \left( \frac{\partial^2 V}{\partial X^2} + \frac{\partial^2 V}{\partial Y^2} \right) - \frac{\text{Pr}}{\text{Da}} V + \text{Pr} \text{Ra} \theta + \text{Ha}^2 \text{Pr} V \quad (3)$$

$$X = \frac{x}{L}, \quad Y = \frac{y}{L}, \quad U = \frac{u \cdot L}{\alpha}, \quad V = \frac{v \cdot L}{\alpha}, \quad P = \frac{pL^2}{\rho\alpha^2},$$

$$\theta = \frac{T - T_0}{T_i - T_0}, \quad \text{Ra} = \frac{\beta g \Delta T L^3}{\alpha \nu}, \quad \text{Da} = \frac{K}{L^2}, \quad \text{Pr} = \frac{\nu}{\alpha} \quad (10)$$

With the boundary conditions:

$$\left( \frac{\partial^2 \theta}{\partial X^2} + \frac{\partial^2 \theta}{\partial Y^2} \right) = U \frac{\partial \theta}{\partial X} + V \frac{\partial \theta}{\partial Y} \quad (4)$$

Entropy  
Entropy production due to friction

$$S_\psi = \phi_1 \left[ U^2 + V^2 \right] + \text{Da} \times \left[ 2 \left[ \left( \frac{\partial U}{\partial X} \right)^2 + \left( \frac{\partial V}{\partial Y} \right)^2 \right] + \left( \frac{\partial U}{\partial Y} + \frac{\partial V}{\partial X} \right)^2 \right] \quad (5)$$

Thermal gradients:

$$S_\theta = \left[ \left( \frac{\partial \theta}{\partial X} \right)^2 + \left( \frac{\partial \theta}{\partial Y} \right)^2 \right] \quad (6)$$

Diffusion

$$S_C = \phi_2 \left[ \left( \frac{\partial C}{\partial X} \right)^2 + \left( \frac{\partial C}{\partial Y} \right)^2 \right] + \phi_3 \left[ \left( \frac{\partial \theta}{\partial X} \right) \left( \frac{\partial C}{\partial X} \right) + \left( \frac{\partial \theta}{\partial Y} \right) \left( \frac{\partial C}{\partial Y} \right) \right] \quad (7)$$

Magnetic field

$$S_M = \phi_1 \times \text{Ha}^2 \times [U \sin \varphi - V \cos \varphi] \quad (8)$$

$$u(x, 0) = u(x, L) = u(0, y) = u(L, y) = 0$$

$$V(X, 0) = V(X, 1) = V(0, Y) = V(1, Y) = 0$$

$$\theta(X, 0) = 1, \quad \text{or}, \quad \theta(X, 0) = \sin(\pi X), \quad \frac{\partial \theta}{\partial Y}(X, 1) = 0 \quad (11)$$

$$\theta(0, Y) = 1\theta(0, Y) = \sin(\pi Y), \theta(1, Y) = 0$$

Thermophysical properties of Al<sub>2</sub>O<sub>3</sub>-Cu/water are presented in Table 1. Those properties are expressed as

The diffusion coefficient is given by [24]:

$$\sigma_{\text{hnf}} = (1 - \varphi)\sigma_f + \varphi\sigma_{\text{np}} \quad (12)$$

The density of nanofluid is given by [23]:

$$\rho_{\text{hnf}} = (1 - \varphi)\rho_f + \varphi\rho_{\text{np}} \quad (13)$$

The thermal expansion coefficient [23]:

$$(\rho\beta)_{\text{hnf}} = (1 - \varphi)(\rho\beta)_f + \varphi(\rho\beta)_{\text{np}} \quad (14)$$

**Table 1** Thermophysical properties of (Cu-Al<sub>2</sub>O<sub>3</sub>/water (50/50) [29]

	$\rho/\text{kg m}^{-3}$	$k/\text{W m}^{-1} \text{K}^{-1}$	$\Sigma/\Omega^{-1} \text{m}^{-1}$	$\beta/\text{K}^{-1}$	$C_p/\text{J kg}^{-1} \text{K}^{-1}$
Pure water	997.1	0.613	$5.5 \times 10^{-6}$	$21 \times 10^{-5}$	4179
Cu	8933	401	$59.6 \times 10^{-6}$	$1.67 \times 10^{-5}$	385
Al <sub>2</sub> O <sub>3</sub>	3970	40	$2.7 \times 10^{-8}$	$0.85 \times 10^{-5}$	765

The specific heat capacity can be determined according to Pak and Cho [25]:

$$(\rho c_p)_{\text{hnf}} = (1 - \varphi)(\rho c_p)_f + \varphi(\rho c_p)_{\text{np}} \quad (15)$$

$$\alpha_{\text{hnf}} = \frac{k_{\text{hnf}}}{(\rho c_p)_{\text{hnf}}} \quad (16)$$

Thermal conductivity is defined as (Wasp model) [26]:

$$k_{\text{hnf}} = \frac{k_{\text{np}} + (n - 1)k_f - (n - 1)(k_f - k_{\text{np}})\varphi}{k_{\text{np}} + (n - 1)k_f + (k_f - k_{\text{np}})\varphi} k_f \quad (17)$$

The effective dynamic viscosity based on the Brinkman mode is considered as [27]

$$\mu_{\text{hnf}} = \frac{\mu_f}{(1 - \varphi)^{2.5}} \quad (18)$$

For nanoparticles  $\text{Al}_2\text{O}_3$  and Cu, the properties are obtained [28]:

$$\varphi = \varphi \text{Al}_2\text{O}_3 + \varphi \text{Cu} \quad (19)$$

$$\rho_{\text{np}} = \frac{\varphi \text{Al}_2\text{O}_3(\rho) \text{Al}_2\text{O}_3 + \varphi \text{Cu}(\rho) \text{Cu}}{\varphi} \quad (20)$$

$$(c_p)_{\text{np}} = \frac{\varphi \text{Al}_2\text{O}_3(c_p) \text{Al}_2\text{O}_3 + \varphi \text{Cu}(c_p) \text{Cu}}{\varphi} \quad (21)$$

$$\beta_{\text{np}} = \frac{\varphi \text{Al}_2\text{O}_3\beta \text{Al}_2\text{O}_3 + \varphi \text{Cu}\beta \text{Cu}}{\varphi} \quad (22)$$

$$k_{\text{np}} = \frac{\varphi \text{Al}_2\text{O}_3 k \text{Al}_2\text{O}_3 + \varphi \text{Cu} k \text{Cu}}{\varphi} \quad (23)$$

$$\sigma_{\text{np}} = \frac{\varphi \text{Al}_2\text{O}_3 \sigma \text{Al}_2\text{O}_3 + \varphi \text{Cu} \sigma \text{Cu}}{\varphi} \quad (24)$$

The local and average Nusselt numbers calculation is very interesting. They are calculated by Roy [30]:

$$\text{Nu}_{\text{local}} = \begin{cases} \frac{k_{\text{hnf}}}{k_f} \frac{\partial T}{\partial x} & \text{vertical walls} \\ \frac{k_{\text{hnf}}}{k_f} \frac{\partial T}{\partial y} & \text{horizontal walls} \end{cases} \quad (25)$$

$$\text{Nu}_{\text{average}} = \frac{1}{L} \int_0^L \text{Nu}_{\text{local}} dL. \quad (26)$$

## Validation and grid independency analysis

### Grid analysis

In this paper, Galerkin finite element procedure with penalty parameter is utilized to solve the nonlinear coupled PDEs for flow and temperature distributions. This method consists of converting nonlinear differential equations into a system of integral equations. Uniform quadratic grids were employed in the discretization of the field's solution. To emphasize the grid independency of current solution, a mesh examining method was performed. Nusselt number is obtained for  $\text{Al}_2\text{O}_3$ -Cu/water ( $\varphi = 0.04$ ) with  $\text{Ra} = 10^6$ . The aforementioned elements to develop an understanding of the grid finesse are shown in Table 2, and a grid size of  $176 \times 176$  should be chosen.

### Validation

The Galerkin finite element method was used for discretizing the Navier–Stokes equations. The computational domain is discretized into quadratic elements as shown in Fig. 1b. The verification of the present code is performed by comparing numerically Khanfer [31] and experimentally Krane and Jeseo [32]. They investigated air flow in a cavity. The dimensionless temperature profile is plotted in Fig. 2 showing the very good agreement with a maximum deviation not exceeding 2%. According to Fig. 3, the present results exhibited negligible difference with numerical solutions of Roy [30].

## Results and discussion

This part clarifies the numerical outcomes for the stream function and isotherms lines for various parameters. The impact of control characteristics such as the Ha (0–80), Ra ( $10^3$ – $10^6$ ), Da ( $10^{-5} \leq \text{Da} \leq 10^{-2}$ ), nanoparticle concentration ( $0 \leq \varphi \leq 0.04$ ) and porosity ratio ( $0.1 \leq \varepsilon \leq 0.9$ ). The values

**Table 2** Comparison of  $\text{Nu}_{\text{avg}}$  for different meshes

$\text{Nu}_{\text{avg}}$	Grid			
	$77 \times 77$	$150 \times 150$	$176 \times 176$	$213 \times 213$
$10^3$	3.0996	3.1206	3.1239	3.1273
$10^4$	3.0766	3.0973	3.1007	3.1040
$10^5$	3.2104	3.2312	3.2345	3.2379
$10^6$	3.9927	4.0179	4.0216	4.0253

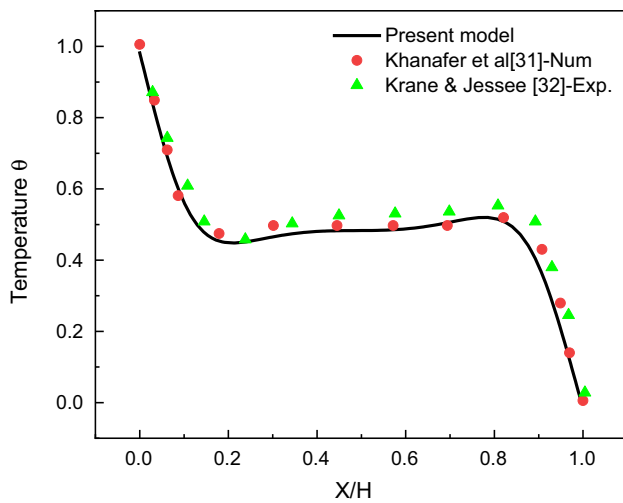


**Fig. 2** Comparison of dimensionless temperature between the current research with numerical solution of Khanafer et al. [31] and experimental findings of Krane and Jesse [32]

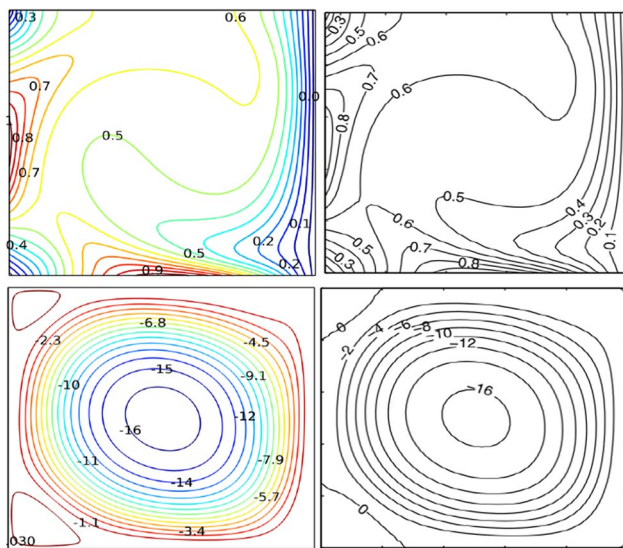


**Fig. 3** Comparison between current data and other studies for the temperature Roy [30]

of the  $Nu_{loc}$  and  $Nu_{avg}$  are also computed for several values of  $Ra$ ,  $Ha$ ,  $Da$ ,  $\epsilon$  and  $\phi$ .

**Stream functions and isotherms**

Figures 4–6 show stream function and isotherms for various parameters with non-uniform heating of a bottom and vertical walls. As expected, the structures of tiny static fluid region are related to the corners of heated vertical wall for the non-uniform heating status. Moreover, for  $Ra = 10^5$  and, due to the current non-uniform heating, the impacts of  $Ha$  on the isotherms profile are also exhibited in these figures. It is noted that the isotherms subject to estimation variations under  $Ha$  boost from 0 to 100 as  $Ra$  enhances. At high  $Ha$ , the conduction transfer mechanism is more obvious. Also, it is seen that the thermal performance becomes stronger with the enhancement of the  $Ra$  while it detracts with the rise in  $Ha$ . Due to the  $Ra$  increase, the flow cell becomes stronger. For  $Ra = 10^6$  and higher Hartmann numbers, the isotherms remain constant which is an indication of convection predominance. The comparison of thermal gradient and total entropy generation for several  $Ra$  is shown in Fig. 7. The isentropic lines show an enhance behavior with enhancing values of various employing parameters except at  $Ha$ .

**Nusselt number**

Figures 8 and 9 display the impact of  $Ra$ ,  $Da$ ,  $Ha$  and the porosity ratio at the heated horizontal ( $X$ ) and vertical walls ( $Y$ ). For the status of great values of  $Ra$ , the thermal performance is very high in both walls. Physically, this kind of conduct is due to the greater values of flow rate in the core of the enclosure. Moreover, for  $Ra = 10^6$  heated walls, the convective regime boosts from the rims across the position with its high value at the position. But for weaker Rayleigh number, ( $Ra = 10^3$ ), the main mechanism is conduction; for this reason there is not much difference for low  $Ra$ . As  $Da$  grows, the medium permeability rises and the convective heat transfer rate boosts.

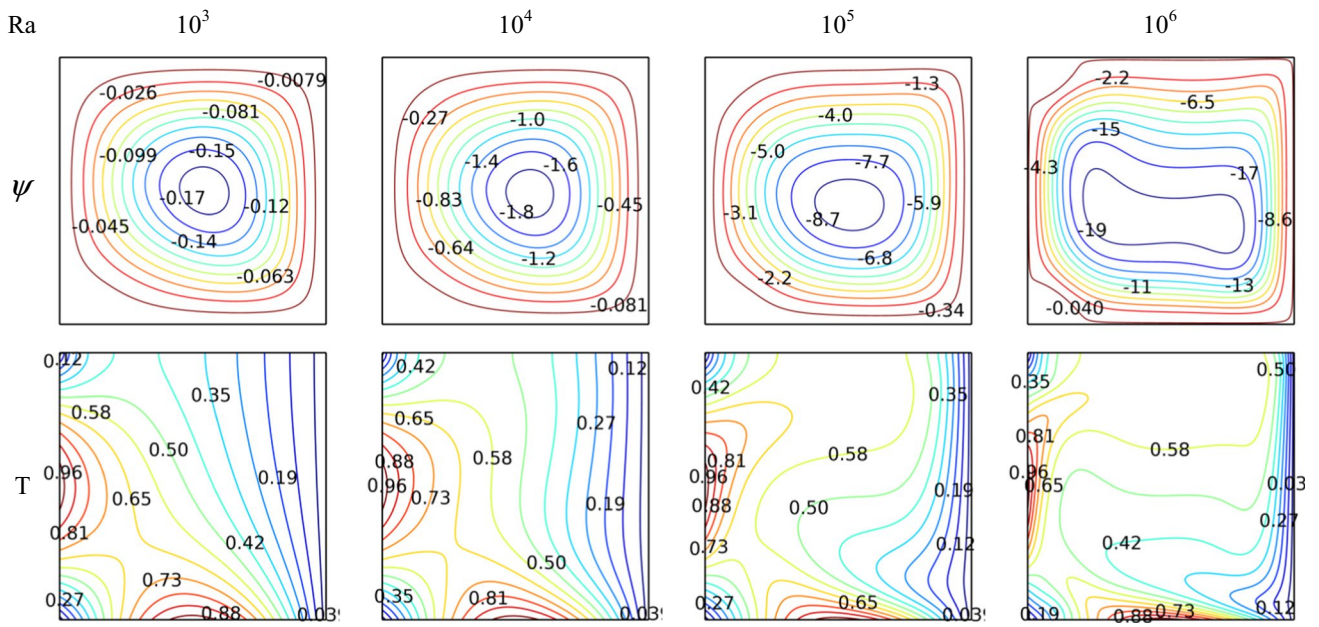


Fig. 4 Isotherm and streamlines for various Ra at Ha=0  $\epsilon=0.4$ ,  $\phi=0.04$

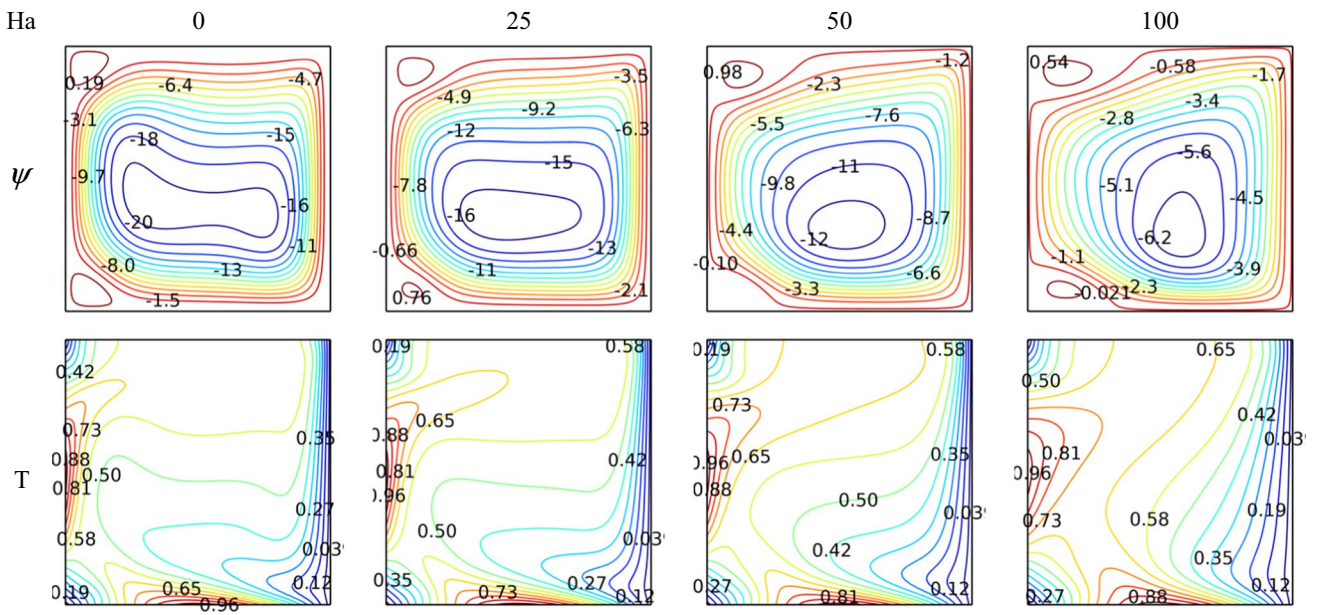


Fig. 5 Isotherm and streamlines for different Ha at Ra=10<sup>6</sup>  $\epsilon=0.4$ ,  $\phi=0.04$

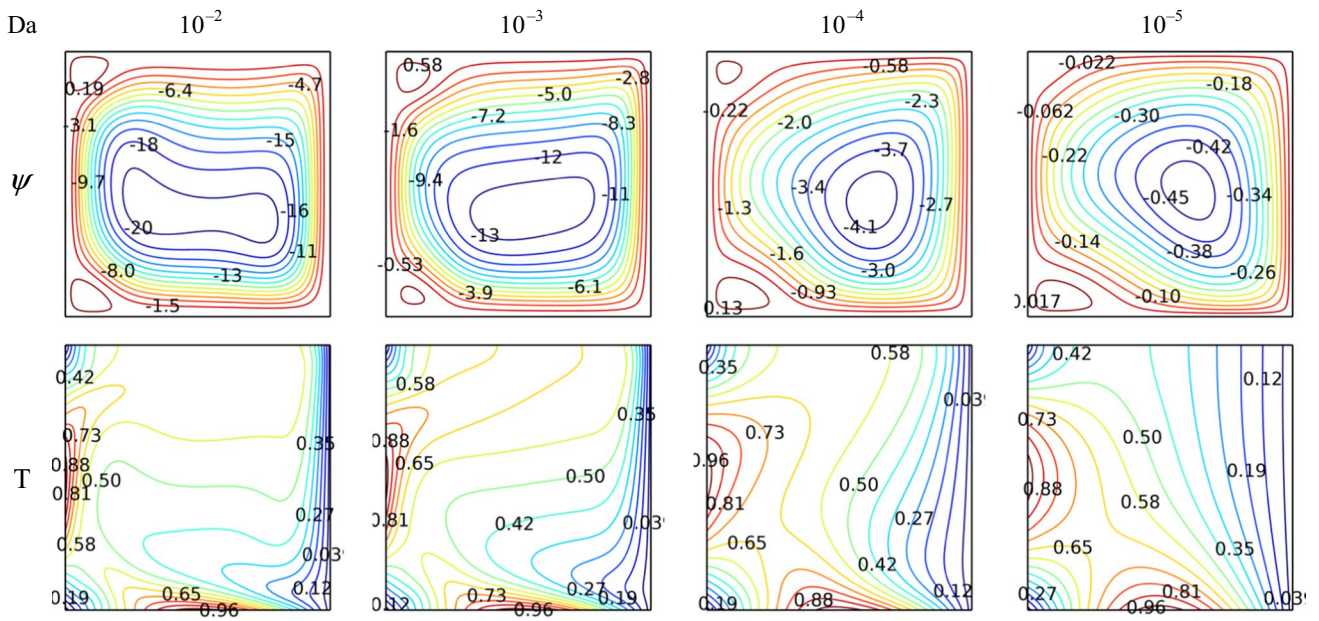


Fig. 6 Isotherm and streamlines for different  $Da$  at  $Ra = 10^6$ ,  $\epsilon = 0.4$ ,  $\phi = 0.04$

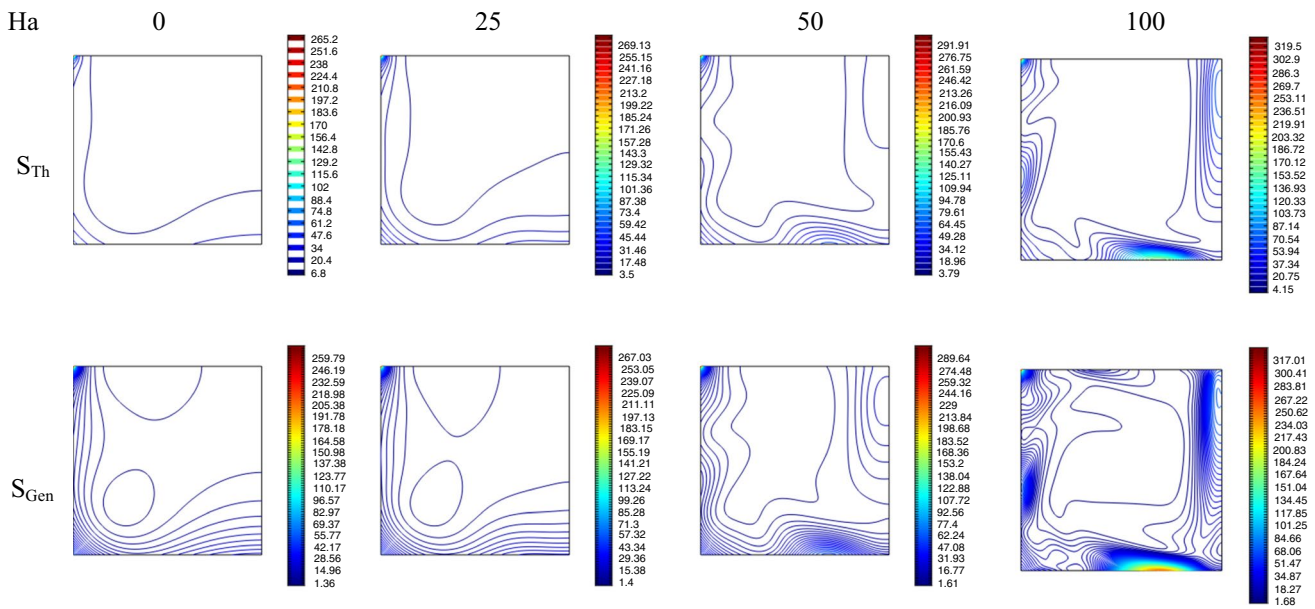


Fig. 7 Thermal gradient and total entropy generation for various  $Ha$  at  $Ra = 10^6$ ,  $\epsilon = 0.4$ ,  $\phi = 0.04$

So, the transfer rate and the absolute values of the flow boost with the rise in Da. As the magnetic strength rises, the Lorentz aspect generates and these strengths decline the velocity of the hybrid nanofluid. Also, the heat transfer declines with the growth in the Ha. It is also appeared that the effect of the hybrid nanoparticles and porosity on the hydrothermal behavior is similar to that of the Rayleigh number.

### Entropy generation

Figure 9 shows the variations of stream function max values, thermal gradient, total entropy generation and average Bejan number for diverse values of Ra and Ha. As we know, Bejan number points out the significance of fluid friction irreversibility and entropy generation due to the transfer heat. It is noticed from Fig. 9 that  $Be_{avg}$  boosts with the decline in the values of Ha, but reduces with the boost in Ra. It is also seen that both the total entropy generation and thermal gradients are increased almost linearly with boosted of Ra and declined Ha numbers (Fig. 10).

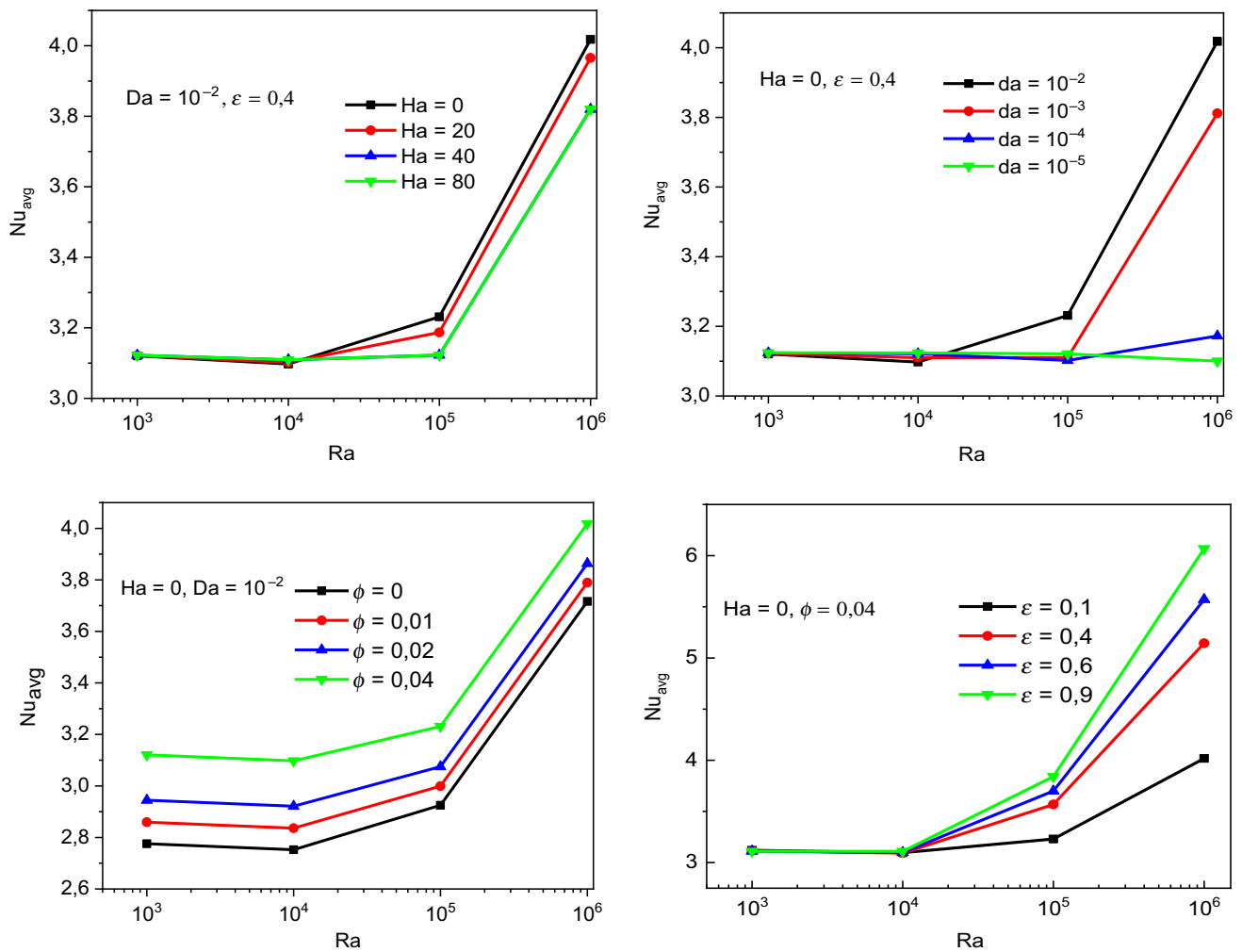


Fig. 8 Nusselt number variation along vertical wall



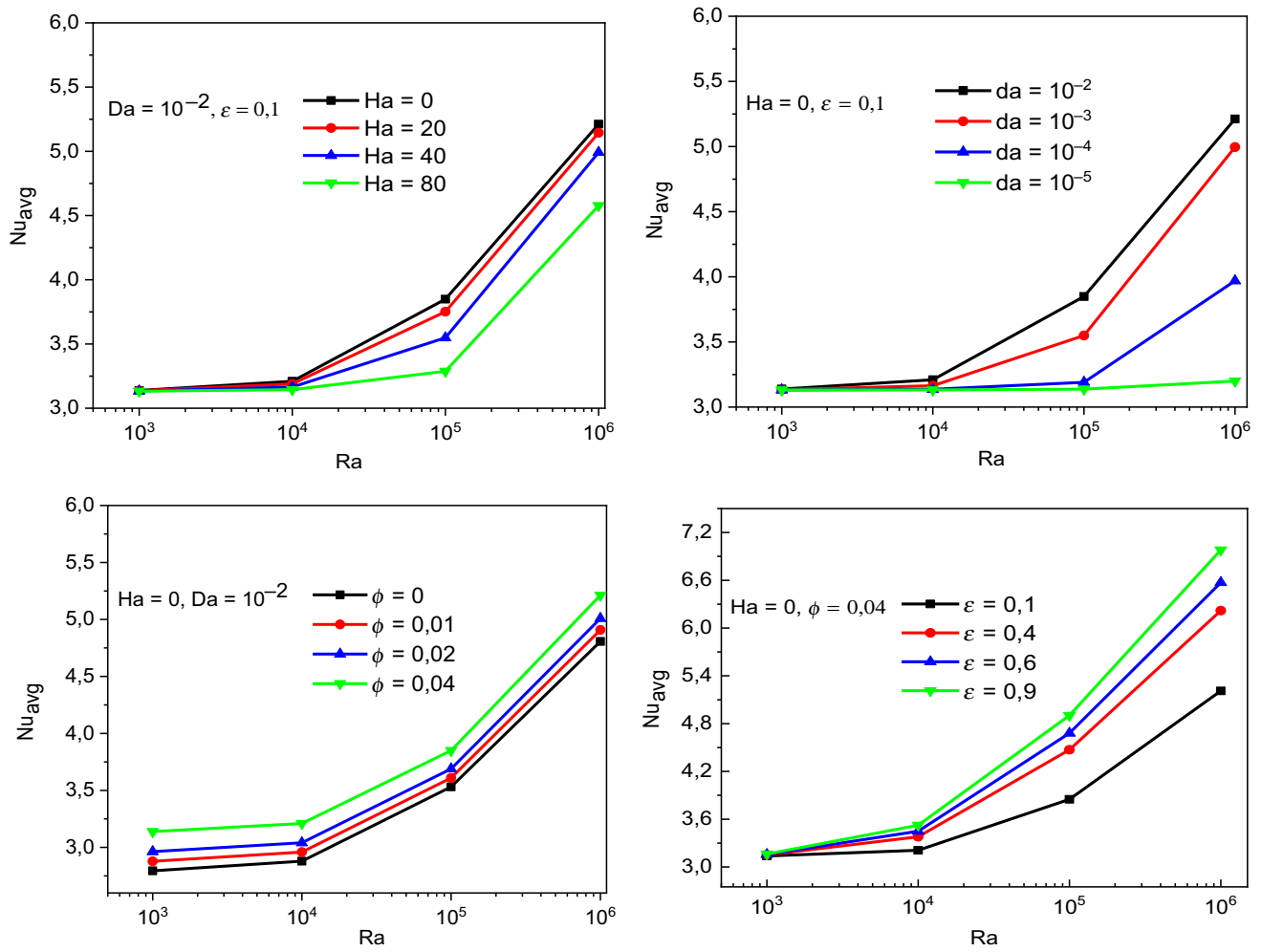
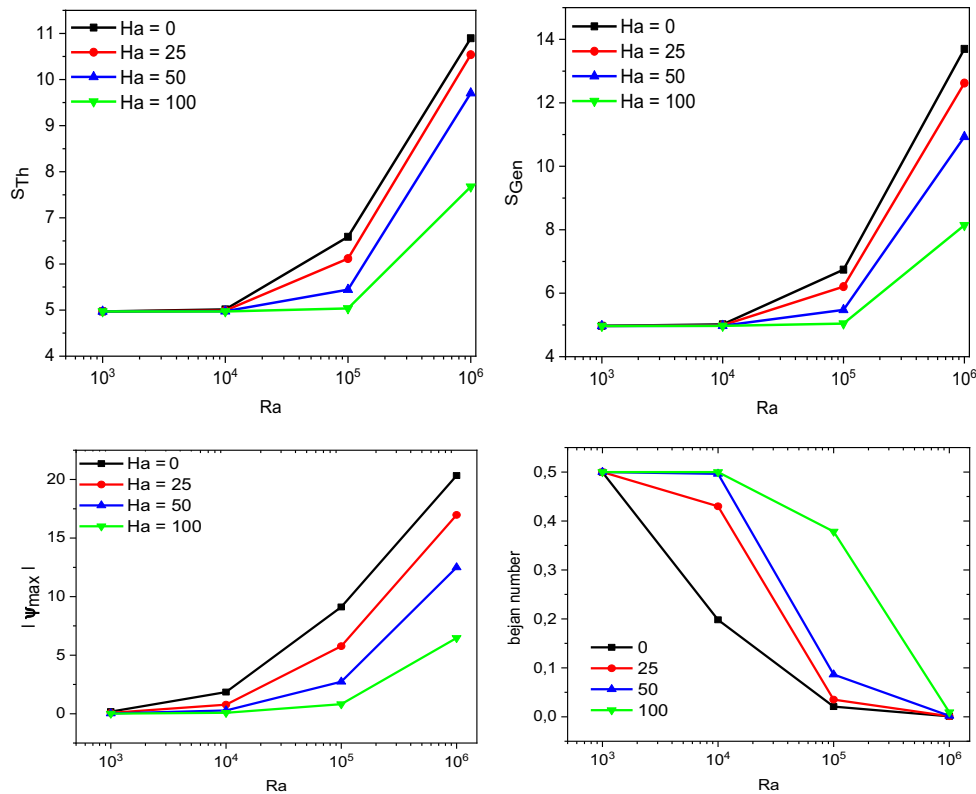


Fig. 9 Average Nusselt number variation along horizontal wall



**Fig. 10** Variations of **a** thermal gradient, **b** total entropy generation, **c** stream function max, **d**  $Be_{avg}$  for different Ra

## Conclusions

In this paper, the numerical investigation of non-uniform heating of the bottom wall and one vertical wall on entropy production during heat transfer convection within a cavity in the presence of magnetic fields was done. The impacts of porosity ratio, nanoparticle concentration and Hartmann and Darcy numbers have been examined. The key findings and conclusions from the current work are as follows:

- the thermal performance increases with the augmentation of Ra,  $\varepsilon$ ,  $\varphi$  and Da and reduces with the enhancement of Ha.
- For the situation of non-uniform heating, the transfer heat is lower at the rims of the heated sides and it reached its maximum value at the center of both heated sides. Also, the sinusoidal kind of changes in transfer heat is noted for non-uniform heating at  $Ra = 10^5$
- The entropy production boosts with growing Rayleigh number, while it declines with Ha
- The influence of permeability of porous medium on entropy production due to transfer heat and fluid friction irreversibility is shown by the local designs of  $S_{th}$  and  $S_{Gen}$ . Due to lower permeability of porous medium at smaller Da, the heat transfer irreversibility is revealed to

predominate the total entropy production in the enclosure.

## References

1. Maghsoudi P, Siavashi M. Application of nanofluids and optimization of the pore size arrangement of heterogeneous porous media to improve mixed convection inside a cavity driven by a two-sided cover. *J Therm Anal Calorim.* 2019;135:947–61. <https://doi.org/10.1007/s10973-018-7335-3>.
2. Mebarek-Oudina F. Convective heat transfer of titania nanofluids of different base fluids in cylindrical annulus with discrete heat source. *Heat Transf Asian Res.* 2019;48:135–47.
3. Siavashi M, Iranmehr S. Using sharp wedge-shaped porous media in front and wake regions of external nanofluid flow over a bundle of cylinders. *Int J Numer Methods Heat Fluid Flow.* 2019;29(10):3730–55. <https://doi.org/10.1108/HFF-10-2018-0575>.
4. Mebarek-Oudina F, Bessaïh R. Numerical simulation of natural convection heat transfer of copper–water nanofluid in a vertical cylindrical annulus with heat sources. *Thermophys Aeromech.* 2019;26(3):325–34.
5. Mahanthesh B, Lorenzini G, Mebarek-Oudina F, Animasaun IL. Significance of exponential space- and thermal-dependent heat source effects on nanofluid flow due to radially elongated disk with Coriolis and Lorentz forces. *J Therm Anal Calorim.* 2019. <https://doi.org/10.1007/s10973-019-08985-0>.

6. Siavashi M, Talesh Bahrami HR, Saffari H. Numerical investigation of porous rib arrangement on heat transfer and entropy generation of nanofluid flow in an annulus using a two-phase mixture model. *Numer Heat Transf Part A Appl.* 2017;71(12):1251–73. <https://doi.org/10.1080/10407782.2017.1345270>.
7. Siavashi M, Rasam H, Izadi A. Similarity solution of air and nanofluid impingement cooling of a cylindrical porous heat sink. *J Therm Anal Calorim.* 2019;135:1399–415. <https://doi.org/10.1007/s10973-018-7540-0>.
8. Asiaei S, Zadehkafi A, Siavashi M. Multi-layered porous foam effects on heat transfer and entropy generation of nanofluid mixed convection inside a two-sided lid-driven enclosure with internal heating. *Transp Porous Med.* 2019;126:223–47. <https://doi.org/10.1007/s11242-018-1166-3>.
9. Siavashi M, Talesh Bahrami HR, Saffari H. Numerical investigation of flow characteristics, heat transfer and entropy generation of nanofluid flow inside an annular pipe partially or completely filled with porous media using two-phase mixture model. *Energy.* 2015;93(2):2451–66.
10. Siavashia M, Talesh Bahrami HR, Aminian E. Optimization of heat transfer enhancement and pumping power of a heat exchanger tube using nanofluid with gradient and multi-layered porous foams Author links open overlay panel. *Appl Therm Eng.* 2018;138:465–74. <https://doi.org/10.1016/j.applthermaleng.2018.04.066>.
11. Raza J, Farooq M, Mebarek-Oudina F, Mahanthesh B. Multiple slip effects on MHD non-newtonian nanofluid flow over a nonlinear permeable elongated sheet: numerical and statistical analysis. *Multidiscip Model Mater Struct.* 2019;15(5):913–31.
12. Reza J, Mebarek-Oudina F, Chamkha AJ. Magnetohydrodynamic flow of molybdenum disulfide nanofluid in a channel with shape effects. *Multidiscip Model Mater Struct.* 2019;15(4):737–57.
13. Mehryan SA, Ghalambaz M, Ismael MA, Chamkha AJ. Analysis of fluid–solid interaction in MHD natural convection in a square cavity equally partitioned by a vertical flexible membrane. *J Magn Magn Mater.* 2017;424:161–73.
14. Talesh Bahrami HR, Safikhani H. Heat transfer enhancement inside an eccentric cylinder with an inner rotating wall using porous media: a numerical study. *J Therm Anal Calorim.* 2020. <https://doi.org/10.1007/s10973-020-09532-y>.
15. Rashad AM, Rashidi MM, Lorenzini G, Ahmed SE, Aly AM. Magnetic field and internal heat generation effects on the free convection in a rectangular cavity filled with a porous medium saturated with Cu–water nanofluid. *Int J Heat Mass Transf.* 2017;104:878–89.
16. Anjali Devi SP, Uma Devi SS. Numerical investigation of hydro-magnetic hybrid Cu–Al<sub>2</sub>O<sub>3</sub>/water nanofluid flow over a permeable stretching sheet with suction. *IJNSNS.* 2016;17(5):249–57. <https://doi.org/10.1515/ijnsns-2016-0037>.
17. Afrand M, Toghraie D, Ruhani B. Effects of temperature and nanoparticles concentration on rheological behavior of Fe<sub>3</sub>O<sub>4</sub>–Ag/EG hybrid nanofluid: an experimental study. *Exp Therm Fluid Sci.* 2016. <https://doi.org/10.1016/j.expthermflusci.2016.04.007>.
18. Aman S, Mohd Zokri S, Ismail Z, Salleh MZ, Khan I. Effect of MHD and porosity on exact solutions and flow of a hybrid casson-nanofluid. *J Adv Res Fluid Mech Therm Sci.* 2018;44(1):131–9.
19. Ghalambaz M, et al. Local thermal non-equilibrium analysis of conjugate free convection within a porous enclosure occupied with Ag–MgO hybrid nanofluid. *J Therm Anal Calorim.* 2019;135:1381–98. <https://doi.org/10.1007/s10973-018-7472-8>.
20. Mehryan SA, Izadi M, Chamkha AJ, Sheremet MA. Natural convection and entropy generation of a ferrofluid in a square enclosure under the effect of a horizontal periodic magnetic field. *J Mol Liq.* 2018;263(1):510–25.
21. Mohebbi R, et al. Natural convection of hybrid nanofluids inside a partitioned porous cavity for application in solar power plants. *J Therm Anal Calorim.* 2019. <https://doi.org/10.1007/s10973-019-08019-9>.
22. Chon CH, Kihm KD, Lee SP, Choi SU. Empirical correlation finding the role of temperature and particle size for nanofluid (Al<sub>2</sub>O<sub>3</sub>) thermal conductivity enhancement. *Appl Phys Lett.* 2005;87:153107. <https://doi.org/10.1063/1.2093936>.
23. Brinkman HC. The viscosity of concentrated suspensions and solutions. *J Chem Phys.* 1952;20:571. <https://doi.org/10.1063/1.1700493>.
24. Medebber MA, Aissa A, Slimani MEA, Retiel N. Numerical study of natural convection in vertical cylindrical annular enclosure filled with Cu–water nanofluid under magnetic fields. *Defect Diffus Forum.* 2019;392:123–37. <https://doi.org/10.4028/www.scientific.net/DDF.392.123>.
25. Pak BC, Cho YI. Pak\_ Experimental heat transfer: a journal of thermal energy generation, transport, storage, and conversion hydrodynamic and heat transfer study of dispersed fluids with submicron metallic oxide particles. *Exp Heat Transf A J Therm Energy Gener Transp Storage Convers.* 1998;11:151–70. <https://doi.org/10.1080/08916159808946559>.
26. Rehman KU, Malik MY, Zahri M, Al-Mdallal QM, Jameel M, Khan MI. Finite element technique for the analysis of buoyantly convective multiply connected domain as a trapezium enclosure with heated circular obstacle. *J Mol Liq.* 2019;2:86. <https://doi.org/10.1016/j.molliq.2019.110892>.
27. Ashorynejad HR, Shahriari A. MHD natural convection of hybrid nanofluid in an open wavy cavity. *Results Phys.* 2018;9:440–55. <https://doi.org/10.1016/j.rinp.2018.02.045>.
28. Pordanjani AH, Vahedi SM, Rikhtegar F, Wongwises S. Optimization and sensitivity analysis of magneto-hydrodynamic natural convection nanofluid flow inside a square enclosure using response surface methodology. *J Therm Anal Calorim.* 2019;135:1031–45. <https://doi.org/10.1007/s10973-018-7652-6>.
29. Ashorynejad HR, Shahriari A. MHD natural convection of hybrid nanofluid in an open wavy cavity. *J Results Phys.* 2018;9:440–55.
30. Roy S, Basak T. Finite element analysis of natural convection flows in a square cavity with non-uniformly heated wall(s). *Int J Eng Sci.* 2005;43:668–80.
31. Khanafer K, Vafai K, Lightstone M. Buoyancy driven heat transfer enhancement in a two-dimensional enclosure utilizing nanofluids. *Int J Heat Mass Transf.* 2003;46(19):3639–53. [https://doi.org/10.1016/S0017-9310\(03\)00156-X](https://doi.org/10.1016/S0017-9310(03)00156-X).
32. Krane R, Jessee J. Some detailed field measurement for a natural convection flow in a vertical square enclosure. In: *Proceedings of the 1st ASME-JSME thermal engineering joint conference, Honolulu, 20–24 March 1983*, pp. 323–329.
33. Gourari S, Mebarek-Oudina F, Hussein AK, Kolsi L, Hassen W, Younis O. Numerical study of natural convection between two coaxial inclined cylinders. *Int J Heat Technol.* 2019;37(3):779–86. <https://doi.org/10.18280/ijht.370314>.
34. Laouira H, Mebarek-Oudina F, Hussein AK, Kolsi L, Merah A, Younis O. Heat transfer inside a horizontal channel with an open trapezoidal enclosure subjected to a heat source of different lengths. *Heat Transf Asian Res.* 2020;49(1):406–23. <https://doi.org/10.1002/htj.21618>.
35. Mebarek-Oudina F. Numerical modeling of the hydrodynamic stability in vertical annulus with heat source of different lengths. *Eng Sci Technol.* 2017;20(4):1324–33. <https://doi.org/10.1016/j.jestch.2017.08.003>.
36. Reza J, Mebarek-Oudina F, Makinde OD. Slip flow of Cu–Kerosene nanofluid in a channel with stretching walls using 3-stage lobatto IIIA formula. *Defect Diffus Forum.* 2018;387:51–62. <https://doi.org/10.4028/www.scientific.net/DDF.387.51>.
37. Alkasasbeh M, Omar Z, Mebarek-Oudina F, Reza J, Chamkha AJ. Heat transfer study of convective fin with temperature-dependent internal heat generation by hybrid block method. *Heat Transf*

- Asian Res. 2019;48(4):1225–44. <https://doi.org/10.1002/htj.21428>
38. Bozorg MV, Siavashi M. Two-phase mixed convection heat transfer and entropy generation analysis of a non-Newtonian nanofluid inside a cavity with internal rotating heater and cooler. *Int J Mech Sci.* 2019;151:842–57.
39. Miri Joibary SM, Siavashi M. Effect of Reynolds asymmetry and use of porous media in the counterflow double-pipe heat exchanger for passive heat transfer enhancement. *J Therm Anal Calorim.* 2019;1:6. <https://doi.org/10.1007/s10973-019-08991-2>.

**Publisher's Note** Springer Nature remains neutral with regard to jurisdictional claims in published maps and institutional affiliations.